Microsphere-assisted self-referencing digital holographic microscopy in transmission mode

To cite this article before publication: Vahid Abbasian *et al* 2019 *J. Opt.* in press https://doi.org/10.1088/2040-8986/ab0815

Microsphere-assisted self-referencing digital holographic microscopy in transmission mode

Vahid Abbasian[1], Saifollah Rasouli[1,2] and Ali-Reza Moradi[1,2,3]

[1] Department of Physics, Institute for Advanced Studies in Basic Sciences (IASBS), Zanjan 45137-66731, Iran

[2] Optics Research Center, Institute for Advanced Studies in Basic Sciences (IASBS), Zanjan 45137-66731, Iran

[3] School of Nano Science, Institute for Research in Fundamental Sciences (IPM), Tehran 19395-5746, Iran

E-mail: moradika@iasbs.ac.ir

27 January 2019

Abstract. In this paper, we introduce a self-referencing microsphere-assisted transmission digital holographic microscopy (DHM) system in real-image operating mode. Self-referencing DHM arrangements provide a compact geometry that are temporally stable against environmental vibrations and suitable for the measurement of dynamic specimens such as cells. These advantages may be more pronounced for microsphere-assisted DHM systems. In the real-image mode, unlike the virtual-image mode, the working distance is increased. This, in turn, provides flexibility for insertion of additional elements for enhancement of the image quality, or for other required tasks. The lateral resolution enhancement is similar to the virtual image arrangement and the axial resolution is decoupled from the lateral one. The methodology is discussed theoretically and validated experimentally by conducting DHM experiments on standard micro-objects and aggregation of micro-particles. Our results show that, by the assistance of a rather big size 550 μm silica microsphere, a 10$\times$ microscope objective can resolve the 3D structure of a compact disk. The arrangement may be useful toward having a compact and inexpensive bench-top high-resolution three-dimensional imaging apparatus.

Keywords: Microsphere-assisted microscopy, Digital holographic microscopy, Self-referencing holography

1. Introduction

Digital holographic microscopy (DHM), in transmission mode, provides a non-invasive tool for quantitative three-dimensional (3D) imaging of phase objects such as cells and biomaterials [1, 2, 3, 4], and in reflection mode it is a non-contact and non-destructive technique for surface profile measurement [5, 6]. The reconstruction of the digital holograms is carried out numerically and leads to the whole-field information about the object under investigation. In order to separate out the undiffracted reference beam,

the virtual and the real images at the reconstruction plane, a slight angle between the object and the reference waves is introduced in off-axis holography arrangement. However, these arrangements become highly sensitive to environmental vibrations, employ additional optical elements, and lead to higher noise levels. Instead, self-referencing geometry for interferometric techniques greatly reduces such uncorrelated noises. Various setups to achieve self-referencing geometries are developed, by the use of a Lloyd's mirror [7], a microscope binocular module [8], a glass plate for applying a lateral shearing [9], etc. Furthermore, employing interferometric objectives such as modified Michelson objective [10], Mirau objective [11], and Linnik objective [12] are the other (expensive) possibilities for common-path DHM.

In DHM, similar to classical optical microscopy, the spatial resolution is restricted by the diffraction limit. The lateral resolution, in addition to the dependence on the performance of the imaging system, depends also on the features of the recording sensor and the spatial frequency windowing within the numerical reconstruction process [13]. The axial resolution is defined by the sensitivity of the detection system to optical path length changes. Optical super-resolution imaging due to its application benefits in many areas of biology, medicine, and material sciences has seen increasing global interest and rapid growth. Some of the super-resolution approaches approaches are based on the use of near-field optics [14]. The main far-field approaches include stimulated emission depletion microscopy, stochastic optical reconstruction microscopy, photo-activated localization microscopy, Fourier ptychographic microscopy, and structured illumination microscopy [15]. Moreover, simple geometrical super-resolution methods, based on exchanging the degrees of freedom of the imaging system, such as the object's shape and temporal behavior, wavelength behavior, dimensions, and polarization, have been applied for synthetic increasing of the numerical aperture (NA)[16, 17]. Synthetic increasing of the effective NA through geometrical super-resolution methods may be extended to be similarly applied for super-resolution and field-of-view extension in DHM [18].

In the last few years, a simple super-resolution method utilizing a transparent microsphere (MS) has shown promising experimental results [19, 20, 21, 22]. Several aspects of the method have been studied and detailed theoretical investigations have been provided to model the methodology [23, 24, 25, 26, 27]. Super-resolution imaging by the MS approach has also been extended to DHM for quantitative phase contrast imaging and surface profilometry [28, 29, 30, 31, 32]. The improvement in the resolution and the final magnification of the MS-assisted imaging system depends on the relative distance between the MS and the objective and the size and refractive index of the MS [29]. The resolution can be further enhanced if the MS-assisted DHM is combined with structured illumination technique [33, 34, 35] or oblique illumination technique [36, 37].

In this Letter, we present a compact, vibration immune, and high resolution MS-assisted DHM arrangement for transparent objects such as biological specimen.

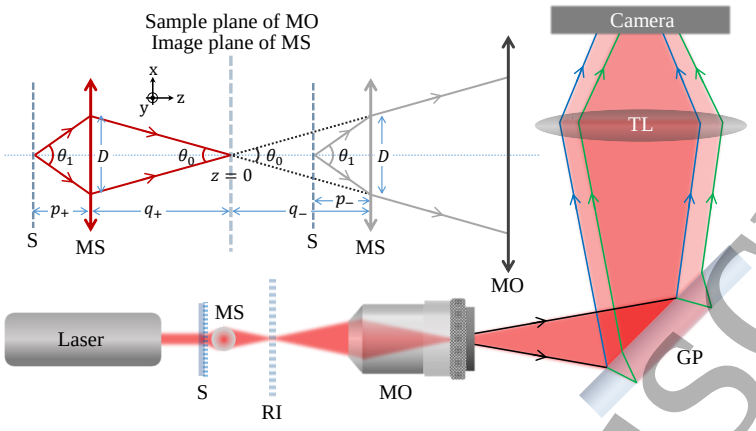

Figure 1. Scheme of the MS-assisted self-referencing DHM in transmission mode setup; S: sample; MS: microsphere; RI: Real image; MO: Microscope objective; GP: Glass plate; TL: Tube lens. Inset: Image formation procedure.

2. Experimental Setup

The scheme of the system is shown in Fig. 1. The collimated He-Ne laser beam (Pooyafarazma, 632.8 nm, 2 mW) illuminates the sample (S) and the diffracted light from the sample is transmitted through the MS. We have used Silica microspheres of 250 μm and 550 μm diameters. The diffracted wave, which includes the high spatial frequencies of the object, is carried by the microsphere, and then the microscope objective (MO, Nikon, NA=0.3, 10x) produces a magnified image of the object. One of the easiest ways to implement self-referencing geometry is the use of a glass plate (GP) to create two laterally sheared replicas of the object wavefront and then superposing them. Two beams follow the same path and go through the same set of optical elements, reducing the unwanted vibrations in the setup. The interference patterns of the sheared wavefronts, containing sample phase information, are recorded by the digital camera (DCC1545M, Thorlabs, 8 bit dynamic range, 5.2 μm pixel pitch) and are subjected to numerical reconstruction process. The shearing applied to the object beam by the use of a GP can be alternatively applied by the use of a proper grating [38]. In a shearing based self-referencing arrangement the sample needs to have object-free regions, which in turn reduces the effective field of view. However, by employing a proper pinhole, one of the interfering object beams can be converted into a separate reference beam providing a similar self-referencing DHM arrangement but with wider field of view [39].

The inset of Fig. 1 shows the image formation protocol in the present setup. When no MS is inserted, the sample is placed at plane $z = 0$ and the scattered beams within the angle θ_0, shown by black dashed lines can enter the optical system and the associated spatial frequencies can be resolved. However, in MS-assisted DHM, two cases may be operated: virtual image mode and real image mode [40]. The gray color beams are the beams originated from the sample, placed at a distance p_- from the MS, and enter into the aperture of the MS. Minus sign stands for the case that the object distance is

below the focal length of the MS. As can be seen, wider light collecting angle (θ_1) can be obtained when an MS is placed in front of the sample. These beams form a bigger virtual image at the sample plane of the the MO at a distance q_- from the MS. In turn, the intermediate virtual image that includes higher magnification and higher spatial frequency acts as an object for the MO. In short, the MO will resolve further details of the sample under study in MS-assisted DHM. In the real image mode, shown by red color beams, however, first the MS forms a real image of the sample (distanced p_+ from the MS) at the sample plane of the MO (distanced q_+ from the MS) and is the same as acts as a sample for the MO. The coverage of the spatial frequencies resolved by the MS-assisted DHM system is almost the same for the two cases, because the collecting angles and the sample-MS distances of the two modes are almost the same; p_- and p_+ values are very close to the focal length of the MS. Therefore, the lateral resolution enhancement of real image is as the one in virtual image arrangement. However, the real image mode comes along with further advantages over virtual mode. In real-image mode, the working distance (WD) unlike the virtual-image mode is increased. Further, the rate of magnification and effective NA variations in the p_+ region is much lower than that of p_- region, hence deeper depth of focus of the system in real mode may be achieved. Thus, the combination of a low magnification MO and an MS in real mode, can be an appropriate alternative for a high magnification MO (which normally has a low WD). Moreover, longer WD provides flexibility for insertion of additional image quality enhancement elements, or for example dichroic mirrors for redirection of fluorescent excitation light if integration of the MS microscopy or MS-assisted DHM with fluorescent microscopy is considered. The difference between the WDs of the two modes ($\Delta\mathrm{WD} = \mathrm{q}_- + \mathrm{q}_+$) depends on the diameter of the MS and the collecting angle of the MO, if the TL and camera positions are remained unchanged; bigger MS leads to lower resolution enhancement and lower WD improvement. However, the final image formation in MS-assisted microcopy depends on the sample axial position with respect to the MS and the MO [29]. Therefore, by adjusting the positions of TL and camera, the position of the MS and hence the resolution and the WD enhancement can be tuned. In the experiment the two modes can be distinguished by following the formed image plane after inserting the MS. If the intermediate image plane, with respect to the no-MS case, is closer to the objective the image is virtual, and if is farther it is a real one. Moreover, real image is direct while the virtual image is inverse (upside-down) and this, additionally, can be used to discriminate the two modes. It should be noted that the theoretical mechanisms for explanation of the MS-assisted microscopy that have been presented for virtual imaging can also be applied to real images.

We have used angular spectrum propagation method [41] to reconstruct the recorded holograms. The numerical reconstruction includes numerically illuminating the recorded digital hologram by the reference wave and propagating the resulted complex wave-field in the Fourier domain. In the Fourier domain the undiffracted reference beam and the conjugate real image are separated out, and different filtering processes may also be applied. Finally, the complex amplitude ($E(x, y)$) at the desired distance from

the hologram plane is obtained by inverse Fourier transform of the propagated complex amplitude. The phase $\phi(x, y)$ and the intensity $I(x, y)$ of the sample are calculated from the complex amplitude $E(x, y)$ as:

$$I(x, y) = |E(x, y)|^2, \tag{1}$$

$$\phi(x, y) = \arctan \frac{\Im[E(x, y)]}{\Re[E(x, y)]}. \tag{2}$$

Eq. 1 gives the intensity image similar to the one of conventional microscopy. However, the additional benefit of DHM is that it enables numerical refocusing of the intensity image at any desired axial distance. For fully-reflective or pure phase objects, the variations of the amplitude are negligible, and the 3D information are embedded within the obtained phase distribution. If the object under study encounters some changes on its shape or refractive index its phase will be varied. The phase difference is related to such changes occurring between two different states of the object under study. For reflective objects the phase distribution leads directly to the changes on the surface height profile of the object. However, for a transparent object undergoing a change in its refractive index, while keeping its physical thickness constant, the phase distribution directly provides the refractive index distribution, and if the refractive index is remained unchanged it provides the object thickness distribution. Therefore, for transparent objects:

$$\phi(x, y) = \frac{2\pi}{\lambda} n(x, y) h(x, y), \tag{3}$$

where $h(x, y)$ is the thickness profile and $n(x, y)$ is the refractive index profile of the sample. For the samples used in this paper the refractive index in the optical path difference is set to a constant. According to Eq. 3, the reconstructed phase map values fall within the range of $[-\pi/2, \pi/2]$, and to recover the original phase distribution of the object, the unwrapping process is applied to the phase map. In this paper, we have used Goldstein's branch-cut unwrapping method to convert reconstructed phase into continuous-phase distributions [42].

In our experiments to remove the effect of possible contaminations and aberrations in the optical train, including the spherical aberration caused by insertion of the MS, we acquired reference holograms, in which the transparent sample was completely removed from the arrangement.

3. Experimental Results and Discussions

In order to prove the capability and usefulness of our approach, first we applied it on a compact disk (CD) after removing its protecting layer, and investigated the various adjustment parameters. Then, we successfully applied the technique to investigate volumetric information of aggregation of micro-spheres and to distinguish the adjacent ones that cannot be resolved without the use of the MS. The results are shown in Figs. 2 and 3. Figure 2(a) shows a recorded digital hologram of a CD and its Fourier

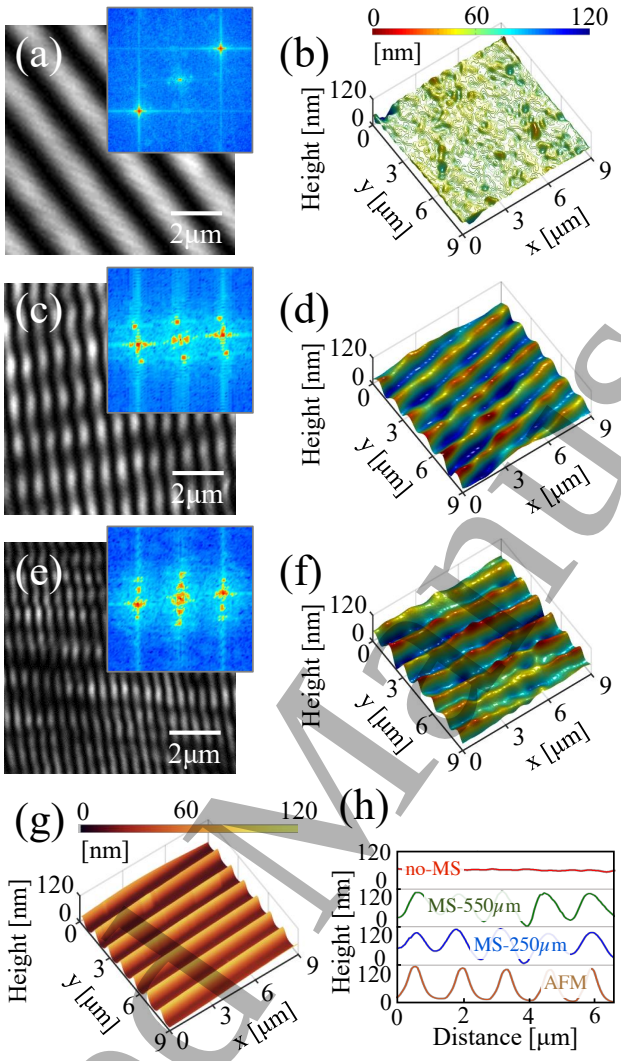

Figure 2. Hologram of a CD, its Fourier spectrum, and the reconstructed 3D image: (a-b) without MS, (c-d) with an MS of 550 μm diameter, and (e-f) with an MS of 250 μm diameter; (g) the corresponding AFM image of the sample; (h) Comparison of cross-sectional profiles.

spectrum in the self-referencing DHM system when no MS was inserted. The numerically reconstructed 3D image is shown in Fig. 2(b), stating that the grooves of the CD structure were not resolved by the DHM system, for vairous windowing procedures that we applied in the Fourier domain. However, with an MS of 550 μm diameter placed between the sample and the MO (Fig. 2(c-d)), without applying any changes in the setup, the structure of the sample is resolved. The side lobes appeared in the Fourier spectrum of the hologram are related to the CD grooves. The 3D image of the sample in which the structure of the CD is clearly resolved is shown in Fig. 2(d). It is known that smaller MSs leads to higher enhancement in the final resolution of MS-assisted microscopies, but reduces the field of view [29]. For the present DHM setup the insertion of smaller MS is helpful for applying proper shearing to the object

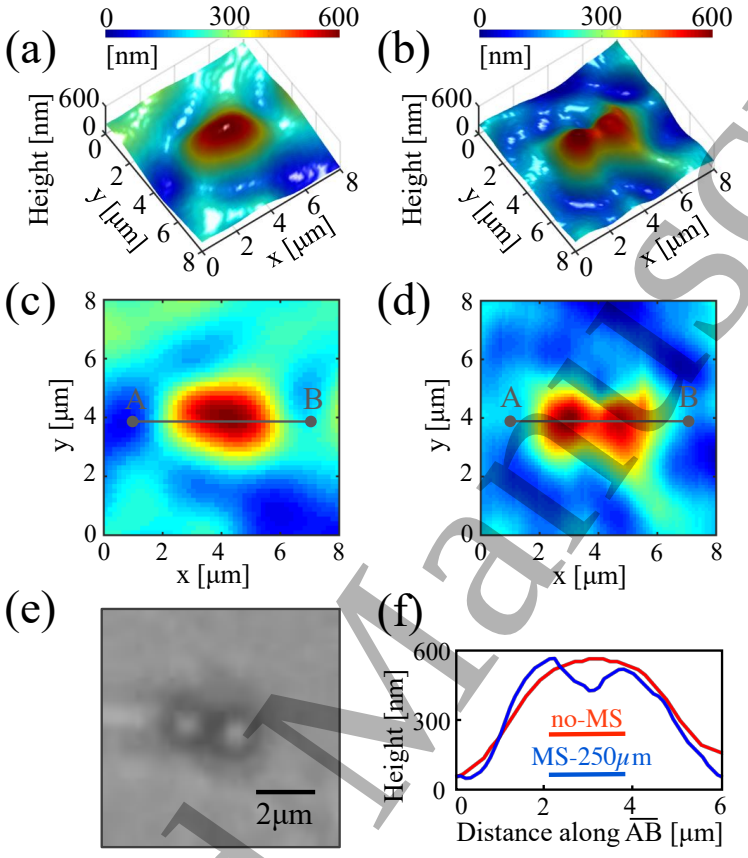

Figure 3. Reconstructed 3D images of two adjacent micro-particles (a) without MS, and (b) with an MS of 250 μm diameter; The corresponding 2D maps (c) without MS, and (d) with the MS; (e) Bright-field microscopy image by a 60× objective; (f) Cross-sectional profiles along the lines $\overline{\text{AB}}$, depicted in panels (c) and (d).

beam; without re-adjusting any elements of the system, the smaller MS produces finer holographic fringes, as can be seen from the hologram by an MS of 250 μm diameter (Fig. 2(e)). The associated 3D height profile is shown in Fig. 2(f). In order to confirm the DHM results, we also acquired AFM image of the sample (Fig. 2(g)). The averaged cross-sectional profiles of the CD structure along the lines perpendicular to the direction of the CD grooves for all the cases, simple DHM image (no MS), DHM images with two different size MSs, and the AFM scanning result are compared in Fig. 2(h), and show a very good agreement. Figure 3 shows the experimental results of polystyrene micro-particles. A 5 μl droplet of diluted dispersed micro-particles of 1.65 μm diameter in polyvinyl alcohol (PVA) solution was taken and placed on a microscope slide. The

slide was left in room temperature for the solution to evaporate. Micro-particles are distributed on the surface randomly. In some cases the particles are close to each other such that they cannot be resolved with low resolution configurations. We have chosen two adjacent micro-particles. Simple DHM cannot distinguish the two particles that are present in the sample as the reconstructed 3D image shows. However, as the 3D image and the 2D maps show, MS-assisted DHM setup can easily identify the two particles. A conventional microscopy image of the particles acquired with a 60× objective which has higher NA is shown in Fig. 3(e), and the cross-sectional profiles along $\overline{AB}$ lines are shown in Fig. 3(f) and demonastrate the capability of MS-assisted DHM to resolve fine structures.

The classic definition of spatial resolution, based on the concept of the point-spread function, can be used for quantitative evaluation of the resolution enhancement introduced by the MS [43]. In our microscopy system, the image plane and the tube lens remain fixed during the experiments, and repositioning of the MS toward the objective allows for a higher magnification factor. On the other hand, this increases the MS collection cone and the complete system's effective NA value. Therefore, the resolution evaluation can be performed by measuring the magnification factor gained by introducing the MS. For the real-image operating mode, as illustrated in the inset of Fig. 1, the magnification factor of the system (given by $\frac{q_+}{p_+}$) is equal to the ratio of the sin of the collecting angle of the MS-DHM to the one in the DHM system without an MS. It has been shown [44, 28] that the amplified factor of the microsphere equals to $\frac{f_{\rm MS}}{f_{\rm MS}-p_+}$, where, p_+ is the distance from the center of MS to the object plane in the real-image mode and $f_{\rm MS}$ is the focal length of the microsphere. For the 250 μm and 550 μm silica microspheres with refractive index of 1.42, the focal lengths are calculated as 420 μm and 930 μm, and magnification factors of 5.5 and 6.5, respectively, when a clear image as well as well-defined holographic fringes were obtained. By choosing a smaller microsphere along with a higher magnification objective, it should be possible to resolve much finer structures. The proper approach for MS-assisted microscopy with small sized microsphere and high magnification factor objectives is to embed the microspheres of higher refractive index inside a solid transparent medium between the sample and the objective.

4. Conclusion

In conclusion, we introduced a self-referencing MS-assisted DHM setup effective for transparent objects which covers a large class of biosamples. The setup is operating in real-image mode that has the benefit of longer WD. The method was discussed by imaging theory and the setup was tested experimentally, by conducting the validating DHM experiments on a CD and aggregation of micro-particles. This arrangement may be useful toward having a compact and inexpensive bench-top high-resolution 3D imaging apparatus. The system has the potential to be easily integrated with structured and oblique illumination approaches to achieve even higher resolution enhancements. In

such systems, similar to conventional microscopy, by inserting a grating or addressing a grating structure onto a spatial light modulator in the path of the object, higher-frequency information of the object are shifted into the recording range and the shifted frequencies are picked up within the numerical reconstruction process of the recorded digital holograms.

Acknowledgments

The authors thank Mr. Jamal Soltani for his assistance in preparation of the samples and Ms. Yasaman Ganjkhani for proofreading the article.

References

[1] Osten W, Faridian A, Gao P, Körner K, Naik D, Pedrini G, Singh A K, Takeda M and Wilke M 2014 *Applied optics* **53** G44–G63
[2] Moon I, Daneshpanah M, Anand A and Javidi B 2011 *Optics and Photonics News* **22** 18–23
[3] Marquet P, Rappaz B, Magistretti P J, Cuche E, Emery Y, Colomb T and Depeursinge C 2005 *Optics letters* **30** 468–470
[4] Mosaviani R, Moradi A R and Tayebi L 2016 *Materials Letters* **173** 162–166
[5] Asgari P, Pourvais Y, Abdollahi P, Moradi A, Khamedi R and Darudi A 2017 *Materials & Design* **125** 109–115
[6] Thiesing B P, Mann C J and Dryepondt S 2013 *Applied optics* **52** 4426–4432
[7] Chhaniwal V, Singh A S, Leitgeb R A, Javidi B and Anand A 2012 *Optics letters* **37** 5127–5129
[8] Ebrahimi S, Moradi A R, Anand A and Javidi B 2014 *Optics letters* **39** 2916–2919
[9] Singh A S, Anand A, Leitgeb R A and Javidi B 2012 *Optics express* **20** 23617–23622
[10] de Groot P J and Biegen J F 2015 A new class of wide-field objectives for 3d interference microscopy *Optical Measurement Systems for Industrial Inspection IX* vol 9525 (International Society for Optics and Photonics) p 95250N
[11] León-Rodríguez M, Rodríguez-Vera R, Rayas J A and Calixto S 2013 *Optics and Lasers in Engineering* **51** 240–245
[12] Guo R, Yao B, Min J, Zhou M, Yu X, Lei M, Yan S, Yang Y and Dan D 2014 *Journal of Optics* **16** 125408
[13] Ferraro P, Wax A and Zalevsky Z 2011 *Coherent Light Microscopy: Imaging and Quantitative Phase Analysis* vol 46 (Springer Science & Business Media)
[14] Betzig E and Trautman J K 1992 *Science* **257** 189–195
[15] Hell S W, Sahl S J, Bates M, Zhuang X, Heintzmann R, Booth M J, Bewersdorf J, Shtengel G, Hess H, Tinnefeld P *et al.* 2015 *Journal of Physics D: Applied Physics* **48** 443001
[16] Mendlovic D 2012 *Optical Superresolution* Springer Series in Optical Sciences (Springer New York) ISBN 9780387347158 URL `https://books.google.com/books?id=0PvqBwAAQBAJ`
[17] Borkowski A, Zalevsky Z, Marom E and Javidi B 2011 *JOSA A* **28** 566–575
[18] Zalevsky Z, Gur E, Garcia J, Micó V and Javidi B 2012 *Optics letters* **37** 2766–2768
[19] Darafsheh A, Walsh G F, Dal Negro L and Astratov V N 2012 *Applied Physics Letters* **101** 141128
[20] Duocastella M, Tantussi F, Haddadpour A, Zaccaria R P, Jacassi A, Veronis G, Diaspro A and De Angelis F 2017 *Scientific reports* **7** 3474
[21] Krivitsky L A, Wang J J, Wang Z and Luk'yanchuk B 2013 *Scientific reports* **3** 3501
[22] Wang F, Yang S, Ma H, Shen P, Wei N, Wang M, Xia Y, Deng Y and Ye Y H 2018 *Applied Physics Letters* **112** 023101
[23] Hoang T X, Duan Y, Chen X and Barbastathis G 2015 *Optics express* **23** 12337–12353
[24] Duan Y, Barbastathis G and Zhang B 2013 *Optics letters* **38** 2988–2990

[25] Sundaram V M and Wen S B 2014 *Applied Physics Letters* **105** 204102
[26] Maslov A V and Astratov V N 2016 *Applied Physics Letters* **108** 051104
[27] Maslov A V and Astratov V N 2017 *Applied Physics Letters* **110** 261107
[28] Wang Y, Guo S, Wang D, Lin Q, Rong L and Zhao J 2016 *Optics Communications* **366** 81–87
[29] Aakhte M, Abbasian V, Akhlaghi E A, Moradi A R, Anand A and Javidi B 2017 *Applied optics* **56** D8–D13
[30] Perrin S, Leong-Hoï A, Lecler S, Pfeiffer P, Kassamakov I, Nolvi A, Hæggström E and Montgomery P 2017 *Applied optics* **56** 7249–7255
[31] Abbasian V, Akhlaghi E A, Charsooghi M A, Bazzar M and Moradi A R 2018 *Ultramicroscopy* **185** 72–80
[32] Kassamakov I, Lecler S, Nolvi A, Leong-Hoï A, Montgomery P and Hæggström E 2017 *Scientific reports* **7** 3683
[33] Ganjkhani Y, Charsooghi M A, Akhlaghi E A and Moradi A R 2017 *Optics Communications* **404** 110–117
[34] Astratov V N, Limberopoulos N I and Urbas A M 2017 Super-resolution microscopy methods and systems enhanced by dielectric microspheres or microcylinders used in combination with metallic nanostructures uS Patent 9,835,870
[35] Bezryadina A, Li J, Zhao J, Kothambawala A, Ponsetto J, Huang E, Wang J and Liu Z 2017 *Nanoscale* **9** 14907–14912
[36] Wang F, Liu L, Yu H, Wen Y, Yu P, Liu Z, Wang Y and Li W J 2016 *Nature communications* **7** 13748
[37] Abbasian V, Ganjkhani Y, Akhlaghi E A, Anand A, Javidi B and Moradi A R 2018 *Journal of Optics*
[38] Rasouli S, Sakha F and Yeganeh M 2018 *Measurement Science and Technology*
[39] Vora P, Trivedi V, Mahajan S, Patel N R, Joglekar M, Chhaniwal V, Moradi A R, Javidi B and Anand A 2017 *Journal of biomedical optics* **22** 126001
[40] Lai H S S, Wang F, Li Y, Jia B, Liu L and Li W J 2016 *PloS one* **11** e0165194
[41] Goodman J W 2005 *Introduction to Fourier optics* (Roberts and Company Publishers)
[42] Gutmann B and Weber H 2000 *Applied optics* **39** 4802–4816
[43] Mansfield S, Studenmund W, Kino G S and Osato K 1993 *Optics letters* **18** 305–307
[44] Allen K W, Farahi N, Li Y, Limberopoulos N I, Walker Jr D E, Urbas A M, Liberman V and Astratov V N 2015 *Annalen der Physik* **527** 513–522